Supplementary Information

Acoustofluidic Separation of Oblate Spheroid from Sphere using Acoustic Radiation Torque and Force

Muhammad Soban Khan,[1] Mushtaq Ali,[1] Yong Bin Bang,[2] Seong Jae Lee[2,*] and Jinsoo Park[1,*]

[1]Department of Mechanical Engineering, Chonnam National University, 77 Yongbong-ro, Buk-gu, Gwangju 61186, Republic of Korea
[2]Department of Polymer Engineering, The University of Suwon, 17 Wauan-gil, Bongdam-eup, Hwaseong, Gyeonggi 18323, Republic of Korea
*Correspondence: Jinsoo Park (jinsoopark@jnu.ac.kr) and Seong Jae Lee (sjlee@suwon.ac.kr)

Acoustic radiation torque

The acoustic radiation torque (ART) (τ_{rad}) acting on an ellipsoid can be expressed as

$$\tau_{rad} = VE_0 Q_{rad}(e_k \cdot e_z)(e_k \times e_z) \quad (1)$$

where V represents the volume of the object, E_0 represents the characteristic energy density of the incident acoustic wave, while Q_{rad} signifies the dimensionless radiation torque efficiency. The vector e_k is the unit vector in the direction of wave propagation k, and e_z is the unit vector along the object's orientation z axis.[1] The characteristic energy density of the incident wave is defined as

$$E_0 = \rho_0 k^2 \emptyset_0^2/2 \quad (2)$$

where ρ_0 is the density of the object, k is the wave number, and $\emptyset_0$ represents the complex amplitude of the velocity potential. The dimensionless radiation torque efficiency Q_{rad} is defined as

$$Q_{rad} = 1 + 3(\xi_0 + 1)\left[2 + \ln\left(\frac{\xi_0 - 1}{2}\right)\right] \quad (3)$$

Where the radial distance is represented by ξ_0. The ART experienced by the ellipsoid is influenced by the interaction between the incident wave and the ellipsoid orientation, as well as the aspect ratio. Specifically, the ART is primarily influenced by the alignment between the major axis (e_z) and the propagation direction of the incident wave (e_k). The orientation angle (θ_k) of the wave propagation direction is determined from

$$cos\theta_k = e_k \cdot e_z \quad (4)$$

The ART acting on an ellipsoid displays unique characteristics depending on the angle θ_k between the e_k and the e_z. When the incident wave travels along the major axis (θ_k= 0, π),

causing end-on incidence, or when it is perpendicular to the major axis ($\theta_k = \pi/2$), resulting in broadside incidence, the ART is zero due to the axial symmetry of ellipsoid and its orthogonal alignment with the wave. Conversely, at other orientation angles, the ellipsoids within the acoustic field experience the ART, leading to tumbling and subsequent alignment of the ellipsoids.

Wave scattering plays a crucial role in particle separation by exploiting the geometric differences between oblate and spherical particles. Oblate particles, due to their asymmetric shape, experience complex scattering patterns when exposed to acoustic waves. This uneven distribution of scattered waves causes greater lateral forces on oblate particles, making them more susceptible to both acosutic radiation force (ARF) and ART. These forces result in higher deflection and rotation for oblate particles, altering their trajectory more significantly than spherical particles, which scatter waves uniformly and experience less pronounced forces. Additionally, the larger surface area of oblate particles enhances wave particle interactions, further increasing the scattering effects compared to spherical particles of equal volume. Moreover, since the interaction between wave fields and particle geometry is nonlinear, small changes in the magnitude of the acoustic field can have amplified effects on oblate particles, making them highly tunable for selective separation. This principle allows for the optimization of separation techniques in complex biological or industrial applications, where particles of varying shapes and sizes need to be efficiently sorted in real-time.

Radiation force function (Y_p)

The radiation force function (Y_p) of an object in an acoustic field can be expressed by

$$Y_p = \left(a/a_{eff}\right)\frac{1}{4}\int_0^{2\pi} |f_\infty(k,\theta)|^2(1 - cos\theta)d\theta \quad (6)$$

where a is the object radius in the major axis,

$$a_{eff} = \sqrt{(a^2 + b^2)/2} \quad (7)$$

is the effective radius, b is the object radius in the minor axis, and

$$|f_\infty = (k,\theta)| \quad (8)$$

represents the magnitude of the backscattering. The ARF function describes the force exerted on the object by the incident acoustic wave. The ARF is generated by the momentum transfer from the incident wave to the object due to scattering and interference effects. The backscattering term in **Equation 8** is directly proportional to the ARF, as a greater magnitude of backscattering indicates a more substantial momentum transfer from the incident wave to the object, leading to an increased ARF.[2]

Numerical investigation of asymmetric wave scattering from oblate spheroids with varying orientation and aspect ratio

Fig. 2a illustrates a numerical model of a rigid ellipsoid exposed to an incident plane progressive wave, referred to as the background pressure field P_b, to simulate wave scattering from both spherical and oblate particles. The ellipsoid is positioned within a computational domain of radius R_i, surrounded by a perfectly matched layer (PML).[3] The semi-axes of the ellipsoid are defined as x, y, and z, with p representing the scattered field from the object. This model, constructed and simulated using COMSOL Multiphysics 6.0, explores the scattering behavior of acoustic waves. At a distance of R_{ext} = 100 μm beyond the computational domain, the scattered field is calculated, allowing the separation of the incident pressure field from the scattered one. The total acoustic field, p_t is given by

$$p_t = p_0 e^{-i(k \cdot x)} + p, \tag{9}$$

which sums the scattered and background fields, where p_0 is the wave amplitude, $\boldsymbol{k}$ is the wave number $\boldsymbol{k} = 2\pi f_0/c_0$, f_0 is the acoustic frequency, and c_0 is the speed of sound. Water at 22°C, the same as in the experiments, was used as the surrounding fluid medium. After solving the pressure acoustics model, the exterior field calculation feature was employed to compute the pressure outside the computational domain. This feature utilized the Helmholtz-Kirchhoff (H-K) integral, applied to the selected boundaries, which formed a closed surface around all sources and scatterers. The H-K integral has two versions: one calculates pressure at the infinity limit, while the other solves the full integral. In this model, the full H-K integral was used, enabling precise determination of the exterior field pressure, including phase, at any point and distance outside the domain. To visualize this, the exterior-field pressure variable p_{ext} , was defined in the model, representing the pressure at coordinates x, y, and z outside the boundary where the exterior-field calculation was applied. The exterior-field pressure and sound pressure level were easily plotted using radiation pattern plot types. For accurate evaluation, the H-K integral was calculated, and the normal derivative of the pressure on the exterior-field surface was automatically handled by a single boundary layer mesh generated by the physics-controlled mesh.

Acoustic radiation force factor

The ARF factor (F_F) induced by the SAWs is expressed as

$$F_F = \langle F \rangle / \left(\pi d_p^2 \bar{E}/4\right), \tag{10}$$

Where ⟨F⟩ is a time-averaged ARF and Ē is the mean energy density of the incident wave and d_p is the particle diameter. The ARF factor acting on the elastic polymer microparticles as a function of Helmholtz number (κ) can be characterized with several maxima peaks and minima valleys, where each peak is attributed to a resonance mode of the freely vibrating elastic microsphere subjected to an oscillating acoustic pressure field.[4]

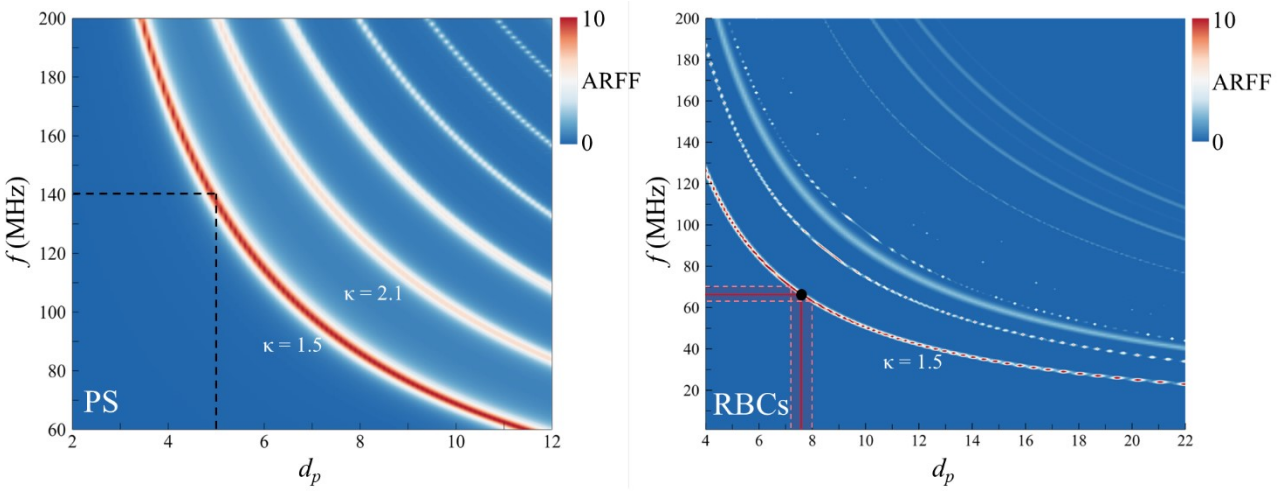

Fig. S1: Contour plot showing the acoustic radiation force factor (F_F) with varying acoustic wave frequency (f) and the PS particle and RBCs diameter (d_p).

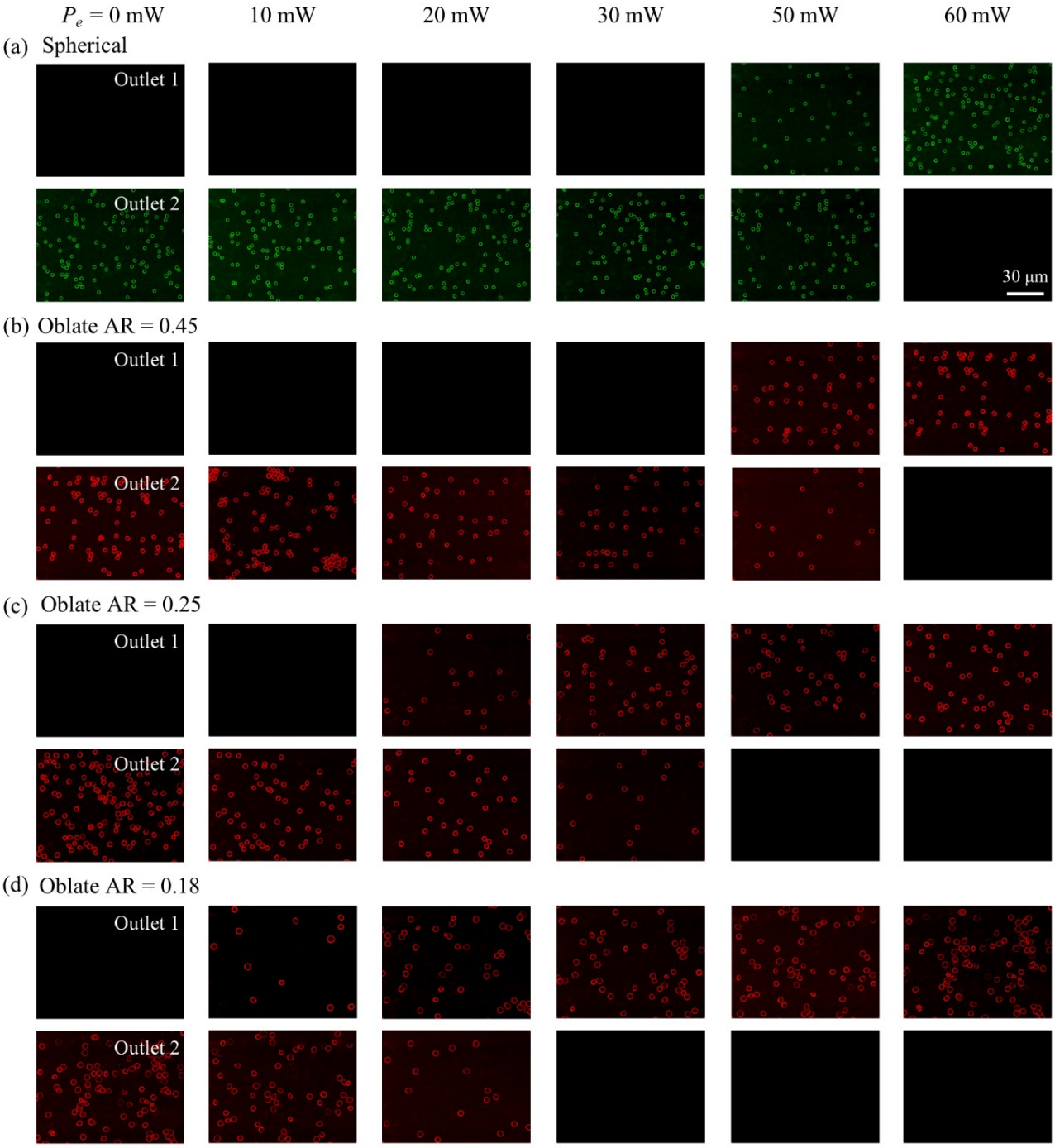

Fig. S2: Collection of spherical and oblate PS microparticles at the two outlets after sorting experiments: a) Microspheres, b) Oblate particles with AR = 0.45, c) Oblate particles with AR = 0.25, and d) Oblate particles with AR = 0.18.

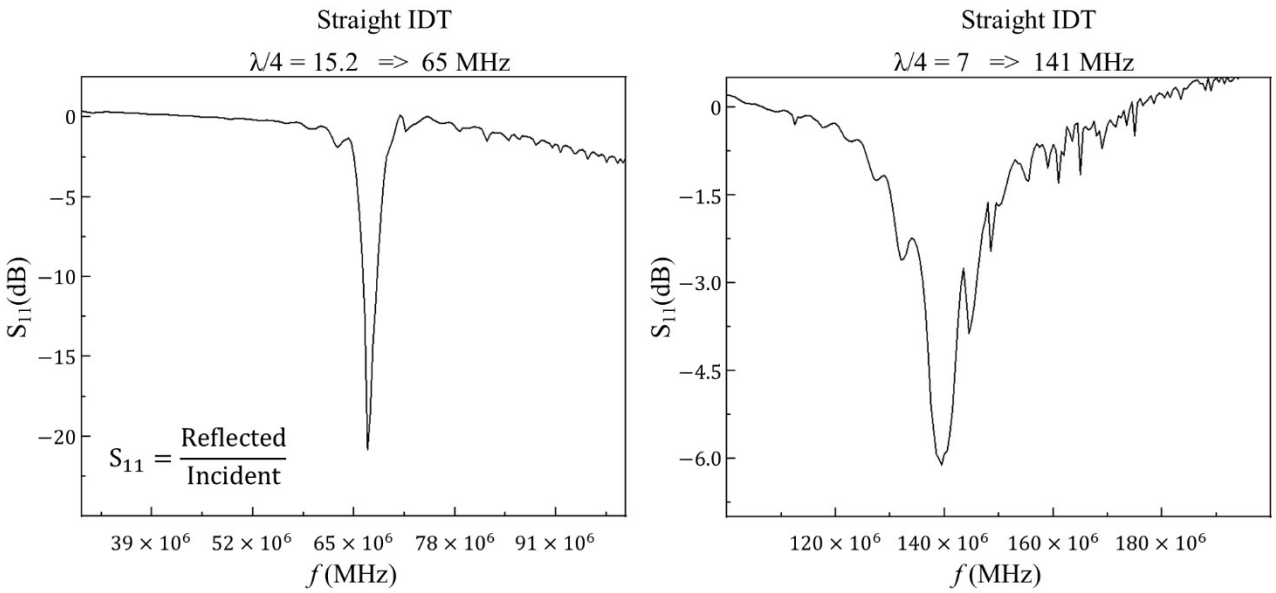

Fig. S3: S_{11} measurement data of both IDTs by a vector network analyzer.

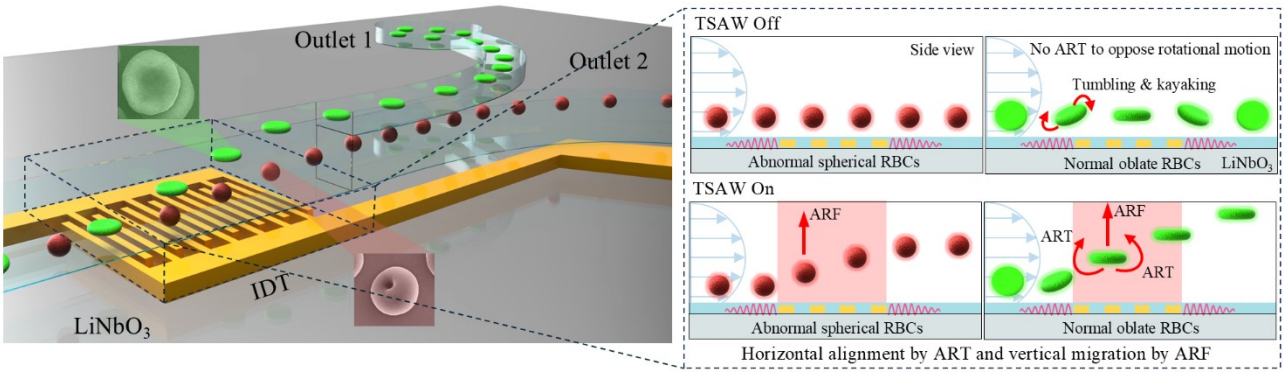

Fig. S4: Roles of ART and ARF in particle orientation and particle vertical migration.

TABLE. 1: Quantitative metrics for shape-based separation of oblate and spherical particles (Figure 8).

Power (mW)	Particle Types	Purity (%) (Outlet 1 / Outlet 2)	Recovery Rate (%) (Outlet 1 / Outlet 2)	Throughput (cells/s)
30 mW	Oblate (AR = 0.18) vs Spherical (5 μm)	100 / 100	100 / 100	
30 mW	Oblate (AR = 0.25) vs Spherical (5 μm)	100 / 92.5	96 / 100	30-40
30 mW	Oblate (AR = 0.18) vs Oblate (AR = 0.45)	100 / 100	100 / 100	

TABLE. 2: Quantitative metrics for shape-based separation of normal and abnormal RBCs (Figure 10).

Power (mW)	Separation Description	Purity (%) (Outlet 1 / Outlet 2)	Recovery Rate (%) (Outlet 1 / Outlet 2)	Throughput (cells/s)
0 mW	No acoustic separation	0 / 50	0 / 100	
10 mW	Weak/No effective separation	0 / 50	0 / 100	
20 mW	Weak/No effective separation	0 / 50	0 / 100	
				30-40
30 mW	Effective separation begins	100 / 86	90 / 100	
50 mW	Strong separation	90 / 100	100 / 92	
70 mW	Complete separation (reversed outlets)	50 / 0	100 / 0	

References:
[1] Leão-Neto, J. P.; Lopes, J. H.; Silva, G. T., *The Journal of the Acoustical Society of America* **2020,** *147* (4), 2177-2183. DOI 10.1121/10.0001016.
[2] Mitri, F. G., *Physics of Fluids* **2016,** *28* (7). DOI 10.1063/1.4959071.
[3] Bermúdez, A.; Hervella-Nieto, L.; Prieto, A.; Rodrı´guez, R., *Journal of Computational Physics* **2007,** *223* (2), 469-488. DOI https://doi.org/10.1016/j.jcp.2006.09.018.
[4] Khan, M. S.; Sahin, M. A.; Destgeer, G.; Park, J., *Ultrasonics Sonochemistry* **2022,** *89*, 106161. DOI https://doi.org/10.1016/j.ultsonch.2022.106161